Journal of Power Sources Advances 20 (2023) 100113

Contents lists available at ScienceDirect

Journal of Power Sources Advances

journal homepage: www.sciencedirect.com/journal/journal-of-power-sources-advances

The effect of addition of the redox mediator dimethylphenazine on the oxygen reaction in porous carbon electrodes for Li/O_2 batteries

Matthias Augustin [a], Per Erik Vullum [b], Fride Vullum-Bruer [a,c], Ann Mari Svensson [a,*]

[a] Department of Materials Science and Engineering, Norwegian University of Science and Technology (NTNU), Høgskoleringen 1, NO-7491, Trondheim, Norway
[b] SINTEF Industry, NO-7491, Trondheim, Norway
[c] SINTEF Energy, NO-7491, Trondheim, Norway

ARTICLE INFO

Keywords:
Lithium/oxygen (Li/O_2) batteries
Oxygen reduction reaction (ORR)
Gas diffusion electrode (GDE)
Redox mediator
DMPZ

ABSTRACT

Secondary Li–O_2 batteries are promising due to their potentially high theoretical energy density. However, both the discharge (oxygen reduction reaction, ORR) and the recharge reaction (oxygen evolution reaction, OER) are associated with high irreversible losses, and multiple side reactions, depending on the electrolyte of choice. Addition of redox mediators is currently considered a promising route to combat the challenges of the highly irreversible ORR/OER. In this work, the effect of addition of the redox mediator 5,10-dimethylphenazine (DMPZ) on the capacity and reversibility of the oxygen reaction is investigated in porous carbon electrodes. The electrolytes are based on tetraethylene glycol dimethyl ether (TEGDME) as solvent, and either Lithium bis(trifluoromethanesulfonyl)imide (LiTFSI) as salt, or a combination of LiTFSI and $LiNO_3$ salt, alternatively dimethyl sulfoxide (DMSO) as solvent, with LiTFSI salt. The addition of DMPZ results in a significant improvement of the reversibility of the ORR/OER reactions for electrolytes based on LiTFSI in DMSO, and LITFSI + $LiNO_3$ in TEGDME. This is attributed to a depression of the side reactions limiting the recharge reaction in these electrolytes. Post mortem analyses by XRD, SEM, as well as FIB-SEM investigations of cross sections, are used to characterize the products from the side reactions.

1. Introduction

The interest in secondary Li/O_2 batteries has grown rapidly over the past two decades, due to the theoretical high energy density (1700 Wh/kg).

However, for current Li–O_2 batteries the performance is far from satisfactory with respect to cycle life, rate-capability and efficiency. The major challenges are related to the oxygen reactions, for example the insulating discharge products, accompanied by a range of side reactions, leading to products like LiOH and Li_2CO_3, or organic products that block the electrode surface. The side reactions are often induced by intermediates from the oxygen reactions like O_2^-, LiO_2 and $^1O_2$.

The current knowledge of the reaction mechanisms is outlined in an excellent review [1], also including a critical assessment of practically achievable energy densities. Recent research has confirmed that the ORR in Li/O_2 batteries proceeds via two main mechanisms [1]. The first reduction step is common for both mechanisms

$$O_2 + Li^+ + e^- \rightarrow Li^+ + O_2^- \rightarrow LiO_2 \quad (1)$$

The intermediate product, LiO_2, is either found in a solvated state, or as a surface species.

The second step is either the disproportionation of solvated LiO_2 to Li_2O_2, referred to as the solution growth pathway (EC mechanism).

$$2\,LiO_2 \rightarrow Li_2O_2 + O_2 \quad (2)$$

The resulting Li_2O_2 products are typically found as toroid-shaped crystalline particles [1] inside the pores of the carbon electrode. Alternatively, the second reduction step is an electrochemical reduction of the surface superoxide, referred to as the surface growth pathway (EE mechanism).

$$LiO_2 + Li^+ + e^- \rightarrow Li_2O_2 \quad (3)$$

The prevailing mechanism of the ORR depend on the electrolyte properties, specifically the Lewis basicity, as given by the Gutman donor number (DN). Among the most commonly applied organic solvents are dimethyl sulfoxide (DMSO) and tetraethylene glycol dimethyl ether (TEGDME) due to their stability with respect to the components in the system and the necessary potential window [2,3]. DMSO and TEGDME

* Corresponding author.
E-mail address: annmari.svensson@ntnu.no (A.M. Svensson).

https://doi.org/10.1016/j.powera.2023.100113
Received 11 November 2022; Received in revised form 12 February 2023; Accepted 27 February 2023
Available online 9 March 2023

are typical examples of high and low Lewis basicity solvents with DNs of 29.8 kcal/mol and 16.6 kcal/mol, respectively. The surface growth pathway is the dominating mechanism in low DN electrolyte solvent [4,5], like TEGDME. The ORR is dominated by the surface growth mechanism when high DN electrolyte solvents, like DMSO, are used and/or discharge parameters, such as low discharge current densities and low overpotentials, are applied [4]. In spite of the higher initial capacity obtained with DMSO solvents, the reversibility and cycling efficiency is typically very poor, attributed to parasitic reactions, to a large extent caused by singlet oxygen, $^1O_2$ formed during discharge [6,7].

A common electrolyte additive is $LiNO_3$, used both for Li–S and Li–O_2 batteries. For Li–O_2 batteries, $LiNO_3$ has been shown to act as a redox mediator [8–10] through the redox couple NO_2/NO_2^- [11]. NO_2^- is formed through the contact between metallic lithium and the $LiNO_3$ salt, and is oxidized to NO_2 around 3.6–3.8 V NO_2 may act as an oxidizing agent, and was found to oxidize Li_2O_2, forming again NO_2^-. In addition, the higher ionic association strength of the NO_3 anion compared to for example the TFSI anion [8], implies that the DN of NO_3^- is significantly higher than for the TFSI anion, i.e. 11.2 kcal/mol vs 22.2 kcal/mol, respectively [12]. The effect of adding $LiNO_3$ is therefore equivalent to the effect obtained upon an increase in the donor number [13] in i.e. the commonly applied electrolytes like LiTFSI/TEGDME or LiTFSI/DME, which again will favor the solution pathway mechanism. Addition of $LiNO_3$ was also found to reduce the parasitic side reactions of the carbon cathode [13]. Furthermore, additions of $LiNO_3$ is well known to passivate metallic lithium anodes [13,14].

Addition of redox mediators is currently considered one of the most promising means to combat the challenges of the highly irreversible ORR/OER. Redox mediators (RMs) acts as "electron-hole" carriers to facilitate the ORR/OER reactions at the cathode. Discharge RMs should therefore have reduction potentials slightly below the reversible potential of the Li–O2 reaction (2), of 2.96 V, and oxidation RMs slightly above. In addition, RMs should have good transport properties and stability in the specific system [14,11].

A number of candidate redox mediators have been studied since Chen et al. reported promising results based on tetrathiafulvalene (TTF) in a Li–O_2 cell with $LiFePO_4$ (LFP) as anode [15]. Among frequently studied redox mediators are the reduction mediator 2,5-Di-*tert*-butyl-1,4-benzoquinone (DBBQ) (i.e. for discharge) and the oxidation mediator 2,2,6,6-tetramethyl-1-piperidinyloxy (TEMPO) for charge [16]. Other studies of organic oxidation mediators include various phenothiazines, like 10-methylphenothiazine (MPT) [17,18], *N*-ethylphenothiazine (EPT) [19], *N*-isopropylphenothiazine [20], a series of thiathrene-derived compounds [21], as well as 5,10-dimethylphenazine (DMPZ) [18,20]. Although improved cycling performance and lowering of the oxidation potential has been demonstrated for many redox mediators, a number of side reactions have been reported, i.e. due to reactions with the metallic Li anode, as for MPT [17,22] or deactivation by singlet oxygen for DMPZ in TEGDME [23,23,20]. In a recent study it was shown that the *ortho*-quinone derivative of the DBBQ mediator facilitated the superoxide disproportionation reaction [24], in another DBBQ was combined with vitamin K1 [25], in order to facilitate the superoxide disproportionation. Similarly, the TEMPO mediator has been modified with acetamido functional group [26], which enabled a bifunctionality, i.e. mediation of the oxidation reaction by the TEMPO, and improved superoxide solvation capability by the acetamido moiety. Similar bifunctionality was demonstrated by functionalization of TEMPO by COOH, as the TEMPO-COOH was shown to catalyze the disproportionation of O_2 radicals, while still acting as an oxidation mediator [27]. Malonic acid-decorated fullerene (MA-C60) has recently bee n shown to function as a superoxide disproportionation chemocatalyst [28].

DMPZ was suggested by Lim et al. [18] on the basis of a screening of candidate redox mediators based on ionization energies, assuming that it serves as an appropriate basis for estimates of the oxidation potential of the mediator. Upon addition of DMPZ, the ability of multiple, stable redox cycles in LiTFSI/TEGDME electrolytes in inert model systems with noble metal electrodes (Ar gas and Pt or Au electrodes) was demonstrated. Two oxidation/reduction peaks were identified in the range of 3.2–4.0 V [18] (at 3.26 and 3.8 V, respectively). In LiTFSI/DMSO electrolytes, reversible cycling was also demonstrated for Pt electrodes, but with 3 reduction peaks over a wider window (2.4 V), of which the upper and lower peaks are small. Later studies of the DMPZ mediator have also been conducted in low DN solvents (TEGDME, DEGDME and DME), and have demonstrated deactivation of the mediator after the second oxidation, see e.g. Ref. [20], where oxidation of Li_2O_2 could not be verified in the presence of DMPZ (in LiTFSI/TEGDME electrolyte). Deactivation was attributed partly to singlet oxygen, $^1O_2$. DMPZ has also been shown to undergo demethylation upon oxidation [29].

In Ref. [30], it was shown that the mediators TTF, TEMPO and DMPZ deactivates during cycling in electrolytes based on DEGDME solvents, regardless of the cathode material (carbon vs. Pt), presence of dissolved oxygen or argon, and also regardless of direct contact with metallic lihium anode. Stable cycling for 50 cycles in the presence of DMPZ could only be demonstrated by lowering the oxidation cut-off potential, to i.e. 3.4 V. Similar findings were reported in Ref. [31].

In view of the fact that the solution growth pathway is the dominating mechanism in DMSO solvents, suffering from high oxidation overpotential, and massive side reactions at high voltages, adding an oxidation mediator is expected to have greater benefits in high DN electrolyte like DMSO. In TEGDME electrolytes, on the other hand, amorphous and reactive Li-oxide films are formed on the carbon surface, with an oxidation potential below the first oxidation potential of DMPZ, for example. For this reason we report here on the oxidation redox mediator DMPZ added to electrolytes based on DMSO solvents with LiTFSI salt, dual salt electrolytes based on LiTFSI and $LiNO_3$ in TEGDME, with increased DN number compared to LiTFSI/TEGDME electrolytes. LiTFSI/TEGDME electrolytes are included for comparison. To our knowledge, DMPZ has so far only been studied with model electrodes (Pt) in DMSO solvent, and there are no studies of the effect of DMPZ in high DN solvents, like DMSO and TEGDME with addition of $LiNO_3$, in combination with porous carbon electrodes. In view of the high oxidation potential of DMPZ, and the fact that it reacts with $^1O_2$, we hypothesize that addition of DMPZ will improve the stability of high DN solvents. The massive electrolyte decomposition observed for DMSO [7] is most likely related to formation of $^1O_2$, and also the cause of the high recharge overpotential. The effect on the capacity and reversibility of the oxygen reaction is investigated in porous carbon electrodes over repeated cycles. The electrochemical investigations are supplemented by post mortem analysis by XRD, SEM of the electrode surface, as well as FIB-SEM investigations of cross sections, in order to reveal differences in product formation for the two solvents.

2. Materials and methods

2.1. Electrode preparation, cell assembly and electrochemical measurements

All materials are listed in the Supporting Information. 1 M Li^+ ion-containing mixtures of LiTFSI/DMSO, LiTFSI/TEGDME and (1 $LiNO_3$: 1 LiTFSI)/TEGDME were prepared in a glove box (MBraun) in an Ar atmosphere with <0.1 ppm H_2O and <0.1 ppm O_2 content. 0.01 M DMPZ was added to the respective solutions. Electrodes were fabricated and assembled as described in Ref. [7].

The carbon black loading of the electrodes was 2.59 mg ± 0.15 mg.

2.2. Galvanostatic cycling

Galvanostatic cycling was performed with a discharge/charge current density of $i = 75$ mA g_C^{-1} and limited to 500 mAh/g on discharge, with an upper cut-off of 4.1 V vs. Li/Li^+. Differential capacity plots were obtained from galvanostatic cycling experiments with a resolution of $\Delta E = 0.1$ mV. All measurements were repeated at least three times. Average

values and standard deviations are displayed in the respective figures unless otherwise noted.

2.3. Characterization methods

Details of the SEM and XRD characterization is found in the Supporting Information. Sample preparation for post mortem analysis is described in Ref. [7].

3. Results and discussion

3.1. Discharge

The cycling performance during galvanostatic discharge/charge in the different electrolytes is shown in Fig. 1a). Addition of DMPZ improved significantly the stability of the LiTFSI/DMSO electrolyte, but has only a moderate effect on the cycling performance of the (LiTFSI + $LiNO_3$)/TEGDME electrolyte, and a minor effect on the cycling performance of the LiTFSI/TEGDME electrolyte. The effect of addition of DMPZ is further illustrated in Fig. 1 b), showing the difference in discharge capacity between the electrodes cycled with and without DMPZ. Thus, the influence of the DMPZ redox mediator on the cycling stability is by far the highest in the high DN solvent DMSO, and also more significant in the LiTFSI/TEGDME containing $LiNO_3$. Addition of $LiNO_3$ will increase the DN of this electrolyte, as NO_3^- has a higher donor number than the TFSI anion [12,13].

The corresponding voltage profiles for the first 5 cycles are shown in Fig. 2 a)-f). The improved cycling performance for the DMSO electrolyte upon addition of DMPZ is evident from i.e. the first cycle coulombic efficiency (CE), which increases from around 75%–85%. For all electrolytes, except LiTFSI/TEGDME, the coulombic efficiency decreases over the cycles.

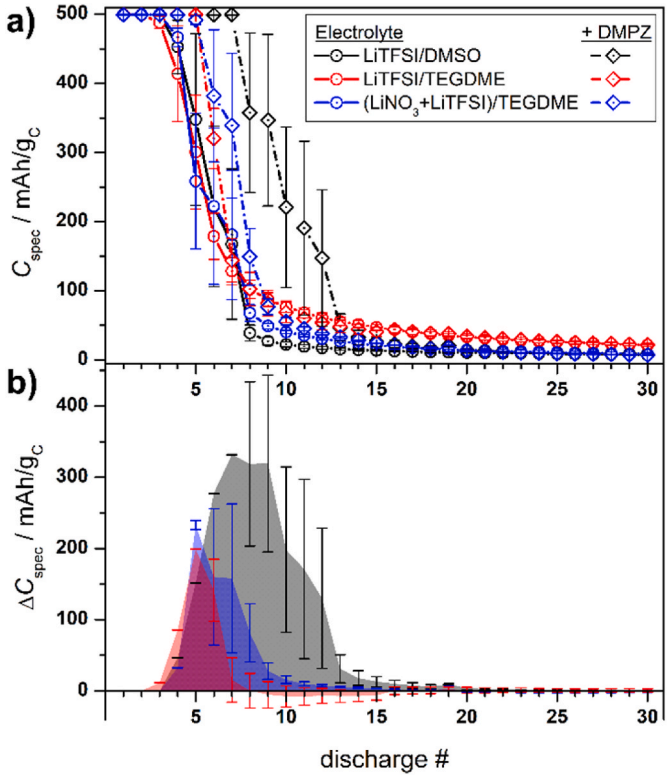

Fig. 1. a) Cycling stability of porous carbon electrodes in LiTFSI/DMSO, LiTFSI/TEGDME and (LiTFSI + $LiNO_3$)/TEGDME electrolytes with and without addition of 10 mM DMPZ at a limited discharge capacity of 500 mAh/g_C. b) The improvement in discharge capacity by adding DMPZ vs. cycle no. for the same electrolytes.

From the voltage profiles, it is observed that the discharge potential of the DMSO electrolyte is higher (2.8 V) compared to the TEGDME electrolyte, around 2.7 V. This is explained by the fact that formation of solvated discharge products, previously shown to be dominating in the high DN DMSO electrolyte [7] has a lower overpotential than the formation of surface discharge products in the low-DN electrolyte (TEGDME). All electrolytes without DMPZ experience a further decrease in the discharge potential after cycle 2 (LiTFSI/TEGDME) and cycle 3 (LiTFSI/DMSO and (LiTFSI + $LiNO_3$)/TEGDME), and they all fail to deliver the capacity of 500 mAh/g_C for the set cut-off potential of 2.5 V.

Upon addition of DMPZ, a constant discharge potential (2.8 V) and discharge capacity (500 mAh/g_C) is observed for the 5 first cycles for DMSO. For both TEGDME electrolytes, there is a small decrease of the discharge potential for cycle 5, but the cathodes are able to deliver the set discharge capacity during the 5 first cycles.

Furthermore, careful inspection of the corresponding differential capacity plots in Fig. 3 shows that for the DMSO electrolyte, one sharp reduction peak is observed at 2.8 V, with a second reduction peak appearing from cycle 4 at a lower potential. Upon addition of DMPZ, there is no sign of a second reduction peak (Fig. 3b)). This second peak indicates the shift from solution mechanism towards the surface mechanism over cycling, as discussed in Ref. [7]. For the LiTFSI/TEGDME electrolyte, the reduction peak is rather broad (in the range 2.65–2.7 V), observed at lower potentials, and independent of addition of the mediator (Fig. 3c) and d)).

Addition of $LiNO_3$ appears to shift the reduction peak towards slightly higher potentials (2.7 V), and the peaks appear similar for the electrolytes with and without DMPZ. Again, this is in agreement with an increase in the DN upon addition of $LiNO_3$, and a shift towards the solution mechanism.

3.2. Recharge

There are significant differences in the recharge behavior between the investigated electrolytes. In brief, for the electrolytes without addition of DMPZ; the DMSO electrolyte exhibit high oxidation potentials due to the formation of crystalline products, and also significant side reactions at high voltages. The amorphous products formed in TEGDME electrolytes are oxidized at lower overvoltages, but also in this solvent there are significant side reaction occurring at high potentials. A detailed comparison of products found during cycling in these two solvents is found in Ref. [7].

Upon addition of DMPZ, the oxidation peaks at ca 3.26 V and ca 3.85 V appear only in the first cycle for all electrolytes, in agreement with other works reporting the deactivation of this compound after the second oxidation [21]. For the subsequent cycles in TEGDME, there is no significant difference between the recharge profiles of the electrodes cycled with and without DMPZ (Figs. 2 and 3). For the DMSO electrolyte it is assumed that the oxidation peak around 3.8 V is related to the oxidation of the crystalline toroids (see Fig. 3 b)). For this electrolyte, the massive side reactions occurring at voltages >3.8 V are not visible in the DMPZ containing electrolyte, even if the redox mediator deactivates, which might explain the improved cycling performance. Recharge in accordance with the solution mechanism prevailing in the DMSO electrolyte is associated with the formation of $^1O_2$. Previous works have shown that DMPZ (and also $DMPZ^+$) is de-activated by the singlet oxygen [32]. Deactivation has been attributed to H-abstraction of the methyl group [33,34]. In this way, the DMPZ acts as a scavenger for $^1O_2$.

Improved passivation is not apparent for the LiTFSI/TEGDME, dominated by the surface film formation during the initial discharge. For the LiTFSI/TEGDME electrolyte, the oxidation reactions at voltages >3.8 appear to be side reactions, which is also consistent with the fact that discharge fails in this electrolyte. Upon addition of DMPZ, oxidation peaks are observed at voltages above 3.8, which could be attributed to either side reactions, or oxidation of DMPZ, in case the deactivation

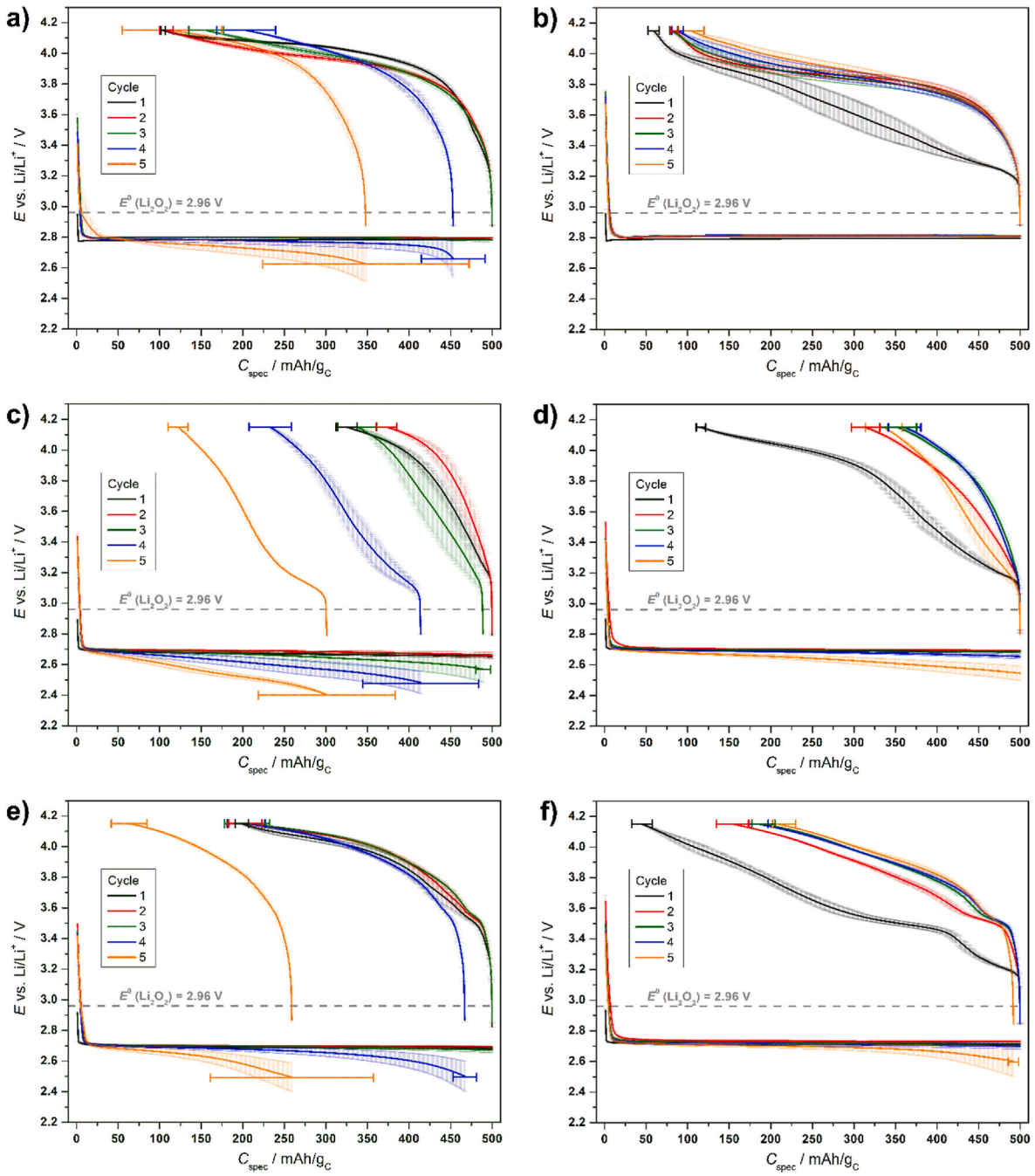

Fig. 2. Voltage profiles for the first 5 cycles obtained for a) LiTFSI/DMSO b) LiTFSI/DMSO +10 mM DMPZ c) LiTFSI/TEGDME d) LiTFSI/TEGDME +10 mM DMPZ e) (LiTFSI + $LiNO_3$)/TEGDME f) (LiTFSI + $LiNO_3$)/TEGDME + 10 mM DMPZ.

occurs over multiple cycles.

For the TEGDME electrolyte with addition of $LiNO_3$ a rather stable oxidation peak is observed around 3.5–3.55 V, in good agreement with the oxidation potential of NO_2^- [8,10], resulting from the reaction between NO_3^- and Li [35,36]. The relatively stable oxidation peaks around 3.9 V (Fig. 3 f)) indicate that toroids are oxidized. By comparing Fig. 3 c) and 3 e), it seems that a more reversible oxidation reaction occurs in the presence of $LiNO_3$, but at a higher potential than for LiTFSI/DMSO. Potential suppression of oxidative damage at the carbon cathode in the presence of $LiNO_3$ has previously been suggested [13].

3.3. Post mortem characterization

SEM micrographs of the electrode surface taken after discharge and recharge in each electrolyte are shown in the Supporting Information, Fig. S1a)-f). From these, characteristic discharge products in the form of toroids are observed in the LiTFSI/DMSO electrolyte (Fig. S1a)), while for the TEGDME, the products appear to be formed as poorly conducting surface films (Fig. S1b)). Reaction products after discharge in the (LiTFSI + $LiNO_3$)/TEGDME electrolyte (Fig. S1c)) are visible inside the pores, consistent with the solution mechanism, but appear rather as disks or platelets, and not as toroids. After recharge, the reaction products have to a large extent been removed for all electrolytes (Fig. S1d)-S1f)), but traces of surface products might still be present. A micrograph of a fresh surface is included as reference in the Supporting Information, Fig. S2a), and cross section of a fresh electrode in Fig. S2b). Cross sections of discharged and recharge electrodes are seen in Figure S3 a)-c) for all electrolytes, and cross sections stitched together in

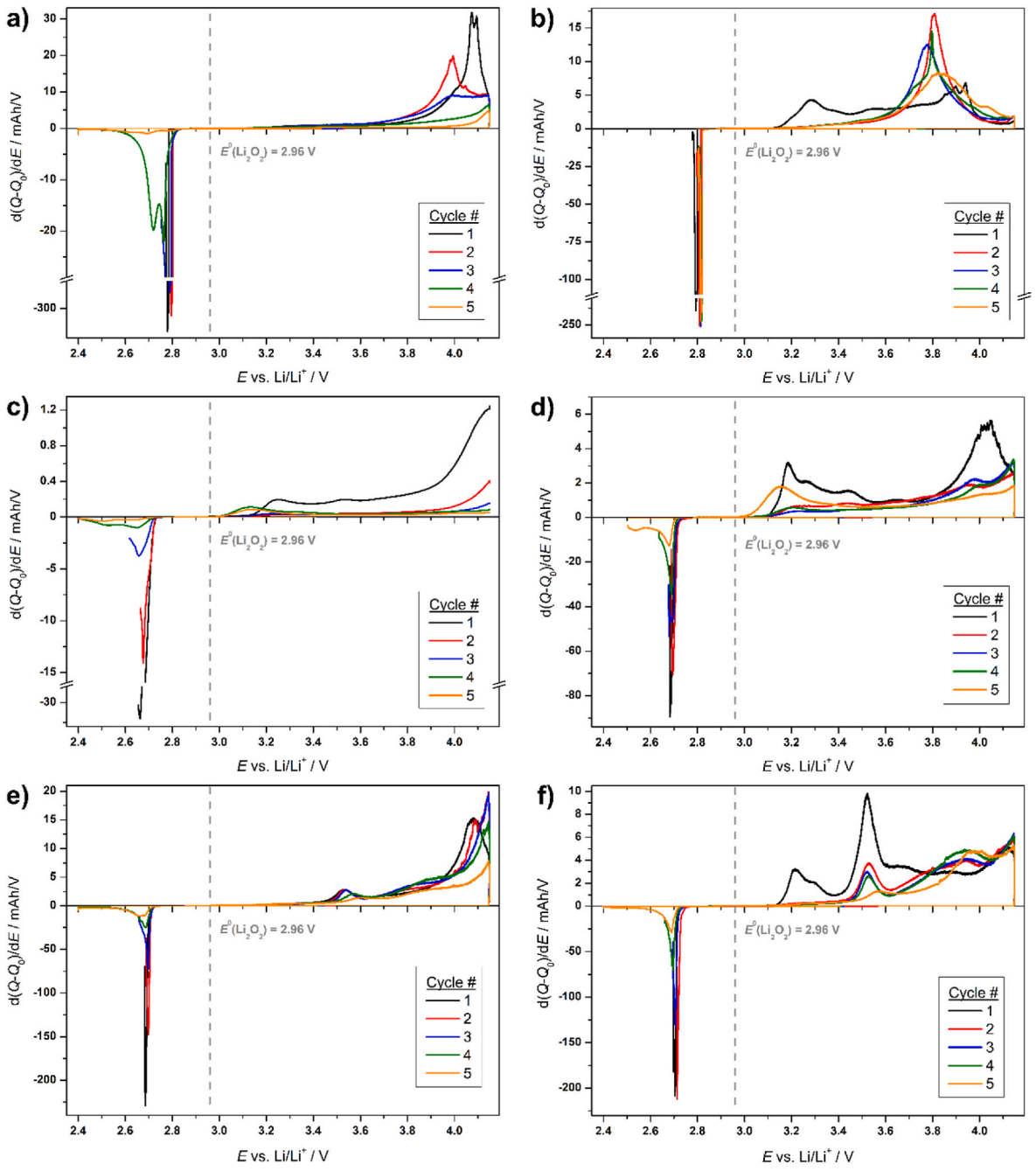

Fig. 3. Differential capacity plot for the first 5 cycles obtained for a) LiTFSI/DMSO b) LiTFSI/DMSO +10 mM DMPZ c) LiTFSI/TEGDME d) LiTFSI/TEGDME +10 mM DMPZ e) (LiTFSI + $LiNO_3$)/TEGDME f) (LiTFSI + $LiNO_3$)/TEGDME + 10 mM DMPZ.

Fig. S4. The cross sections show that the pore structure appears to be more clogged towards the separator for the high DN electrolytes LiTFSI/DMSO and (LiTFSI + LiNO3)/TEGDME, and fails to completely recover upon recharge. For the LiTFSI/TEGDME electrolyte, the pore structure appears more uniform, with less clogging on both discharge and charge. These findings are in line with the previous results, and discussed in more detail in Ref. [7].

SEM micrographs of the electrode surface taken after discharge and recharge in each electrolyte are shown in Fig. 3. From these, characteristic discharge products in the form of toroids are observed in the LiTFSI/DMSO electrolyte (Fig. 3a)), while for the TEGDME, the products appear to be formed as poorly conducting surface films (Fig. 3b)). Reaction products after discharge in the (LiTFSI + $LiNO_3$)/TEGDME electrolyte (Fig. 3c)) are visible inside the pores, consistent with the solution mechanism, but appear rather as disks or platelets, and not as toroids. After recharge, the reaction products have to a large extent been removed for all electrolytes (Fig. 3d)-3f)), but traces of surface products might still be present. A micrograph of a fresh surface is included as reference in the Supporting Information, Fig. S1a), and cross section of a fresh electrode in Fig. S1b). Cross sections of discharged and recharge electrodes are seen in Figure S2 a)-c) for all electrolytes. The cross sections show that the pore structure appears to be more clogged towards the separator for the high DN electrolytes LiTFSI/DMSO and (LiTFSI + LiNO3)/TEGDME, and fails to completely recover upon recharge. For the LiTFSI/TEGDME electrolyte, the pore structure appears more uniform, with less clogging on both discharge and charge. These findings are in line with the previous results, and discussed in more detail in Ref. [7].

X-Ray diffractograms after one discharge cycle in the DMPZ containing electrolytes are shown in Fig. 4, while Fig. 5a) -c) shows the X-Ray diffractograms evolving over time for electrodes disassembled after one discharge, recorded under inert conditions. For comparison, the diffractogram of cycled electrodes for the same electrolytes without DMPZ is provided in the Supporting Information, Fig. S3.

The presence of crystalline Li_2O_2 is clearly visible in the XRD of the GDE after full discharge with (LiTFSI + $LiNO_3$)/TEGDME (Fig. 4). The reflection at 33° and 35° are assigned to the (100) and (101) reflections of Li_2O_2, respectively [25]. Li_2O_2 is only indicated by a weak reflection when using the TEGDME-based electrolyte without $LiNO_3$. Crystalline Li_2O_2 appears to be present also in the LiTFSI/DMSO electrolyte, at a higher intensity than for the TEGDME electrolyte, and with a relatively high intensity of the (100) reflection at 33°.

Fig. 5 shows the evolution of the diffraction peaks for the discharged electrodes, recorded in inert atmosphere over a period of 1000 min. From Fig. 5 a) and b), the presence of LiOH is evident for both the LiTFSI/DMSO and the LiTFSI/TEGDME samples, and for both of these the intensity of the LiOH (011) reflection at around 32.6 °C increase over time. The intensity of the LiOH (011) reflection detected at ca. 32.6° continues to increase after discharge with both LiTFSI/DMSO and LiTFSI/TEGDME, respectively (Fig. 5a) and b)). LiOH is potentially formed upon a chemical reactions between Li_2O_2 and the respective solvent by deprotonation (DMSO) and proton-mediated degradation (TEGDME) [39–41]. Amorphous Li_2O_2 has been found to be more reactive than crystalline Li_2O_2 [4], and amorphous Li_2O_2 is most likely the main product after discharge with the TEGDME-based electrolyte. This is consistent with the evolution of the LiOH peaks. Similarly, the sample with the most crystalline Li_2O_2, observed after discharge ($LiNO_3$+LiTFSI)/TEGDME, is also the sample with only negligible amounts of LiOH (Fig. 5c)).

The XRD results depicted in Fig. 5 also indicate the presence of Li_2CO_3 in the GDE after discharge with all electrolytes, previously also detected as a side product from reactions during cycling [42,43].

4. Conclusion

Addition of the redox mediator DMPZ to electrolytes based on the LiTFSI salt is shown to improve the cycling performance for electrolytes based on the DMSO and TEGDME solvents, as well as for LiTFSI in

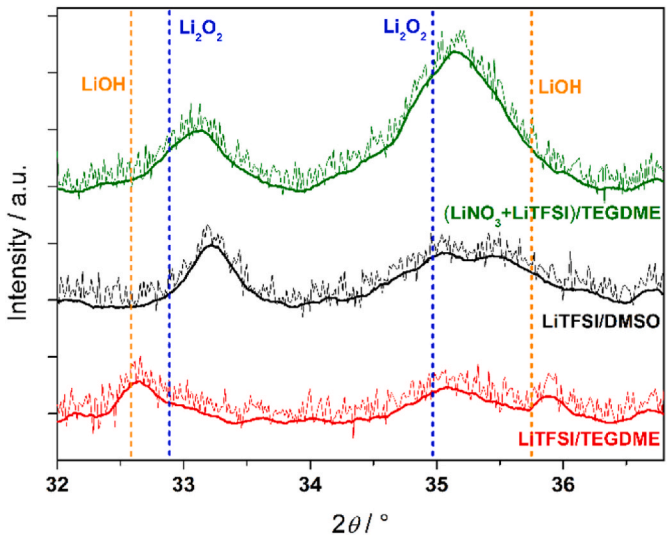

Fig. 4. X-ray diffractogram of the electrodes after the first discharge to 500 mAh/g_C in DMPZ containing electrolytes. Dashed blue and orange lines denote literature reflections of Li_2O_2 [37] and LiOH [38], respectively. (For interpretation of the references to colour in this figure legend, the reader is referred to the Web version of this article.)

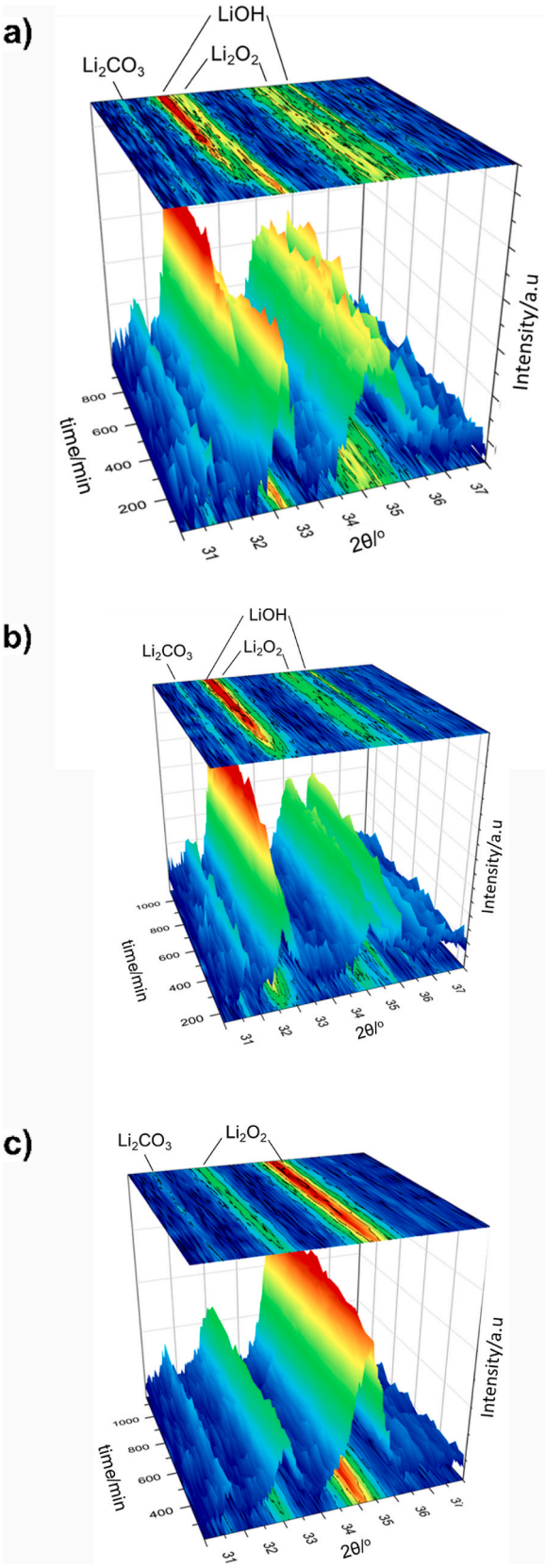

Fig. 5. a) Time-dependent X-ray diffractograms of GDEs after the initial discharge for all electrolytes containing DMPZ for a) LiTFSI/DMSO b) LiTFSI/TEGDME c) and (LiTFSI + $LiNO_3$)/TEGDME.

combination with $LiNO_3$ and TEGDME. The improvement in terms of number of cycles, discharge potential and coulombic efficiency was significant for DMSO, as well as the LiTFSI + $LiNO_3$ in TEGDME, which represent the electrolytes with the highest DN number. All electrolytes showed a deactivation of the DMPZ after the initial cycle, but still the addition of DMPZ led to a significant reduction of side reactions at high overvoltages in the DMSO electrolyte, possibly related to de-activation of singlet oxygen. The transition from the solution mechanism to the surface mechanism is delayed for the DMSO electrolyte with DMPZ.

Declaration of interests

The authors declare that they have no known competing financial interests or personal relationships that could have appeared to influence the work reported in this paper.

Data availability

Data will be made available on request.

Acknowledgments

The Research Council of Norway is acknowledged for the financial support within the framework of the research project “Optimized electrode-electrolyte interfaces for Li-air batteries” (contract number 240 866). The Research Council of Norway is also acknowledged for the support to the Norwegian Micro- and Nano-Fabrication Facility, NorFab, project number 245963/F50.

Appendix A. Supplementary data

Supplementary data to this article can be found online at https://doi.org/10.1016/j.powera.2023.100113.

References

[1] N. Mahne, O. Fontaine, M. Thotiyl, M. Wilkening og S.A. Freunberger, Chem. Sci. 8 (2017) 6716–6729.
[2] M. Trahan, S. Mukerjee, E. Plichta, M.A. Hendrickson og K. Abraham, J. Electrochem. Soc. 160 (2012) A259–A267.
[3] F. Bardé, Y. Chen, L. Johnson, S. Schalti, J. Fransaer og, P. Bruce, J. Phys. Chem. C 118 (2014) 18892–18898.
[4] B. Adams, C. Radtke, R. Black, M. Trudeau, K. Zaghib og L. Nazar, Energy Environ. Sci. 6 (2013) 1772–1778.
[5] N. Aetukuri, B. McCloskey, J. Garciá, L. Krupp, V. Viswanathan og A. Luntz, Nat. Chem. 7 (2015) 50–56.
[6] N. Mahne, B. Schafzahl, C. Leypold, M. Leypold, S. Grumm, A. Leitgreb, C. Slugovc, S. Borisov og S. Freunberger, Nat. Energy 2 (2017), 17036.
[7] M. Augustin, P. Vullum, F. Vullum-Bruer og, A. Svensson, J. Power Sources 414 (2019) 130–140.
[8] D. Sharon, D. Hirsberg, M. Afri, F. Chesneau, R. Lavi, A.A. Frimer, Y.-K.Sun og D. Aurbach, ACS Appl. Mater. Interfaces 7 (2015) 16590–16600.
[9] B. Sun, X. Huang, S. Chen, J. Zhang og G. Wang, RSC Adv. 4 (2014), 11115.
[10] S. Ahn, J. Suk, D. Kim, Y. Kang, H. Kim og D. Kim, Adv. Sci. 4 (2017), 1700235.
[11] V. Pande og V. Viswanathan, ACS Energy Lett. 2 (2017) 60–63.
[12] M. Schmeisser, P. Illner, R. Puchta, A. Zahl og, R. van Eldrik, Chemistry 18 (35) (2012) 10969–10982.
[13] S. Rosy, M. Leskes og M. Noked, ACS Appl. Mater. Interfaces 10 (2018) 29622–29629.
[14] Y. Dou, Z. Xie, Y. Wei, Z. Peng og, Z. Zhou, Natl. Sci. Rev. 9 (2022), nwac040.
[15] Y. Chen, S.A. Freunberger, Z. Peng, O. Fontaine og, P. Bruce, Nat. Chem. 5 (2013) 489.
[16] X. Gao, Y. Chen, L. Johnson, Z. Jovanov og, P. Bruce, Nat. Energy 2 (9) (2017), 17118.
[17] N. Feng, X. Mu, X. Zhang, P. He og, H. Zhou, ACS Appl. Mater. Interfaces 9 (2017) 3733–3739.
[18] H.-D. Lim, B. Lee, Y. Zheng, J. Hong, J. Kim, H. Gwon, Y. Ko, M. Lee, K. Cho og K. Kang, Nat. Energy 1 (2016), 16066.
[19] J. Kowalski, M. Casselman, A. Kaur, J. Milshtein, C. Elliott, S. Modekrutti, N. Attanayake, N. Zhang, S. Parkin, C. Risko, F. Brushett og S. Odom, J. Mater. Chem. A. 5 (2017) 24371–24379.
[20] W.-J. Kwak, J. Park, H. Kim, J. Joo, D. Aurbach, H. Byon og Y.-K. Sun, ACS Energy Lett. 5 (2020) 2122–2129.
[21] P. Arrechea, K. Knudsen, J. Mullinax, J. Haskins, C. Bauschlicher, J.W. Lawson og, B. McCloskey, ACS Appl. Energy Mater. 3 (2020) 8812–8821.
[22] S. Ha, Y. Kim, D. Koo, K.-H. Ha, Y. Park, D.-M. Kim, S. Son, T. Yim og, K.T. Lee, J. Mater. Chem. 5 (2017) 10609–10621.
[23] W.-J. Kwak, H. Kim, Y.K. Petit, C. Leypold, T.T. Nguyen, N. Mahne, P. Redfern, L. A. Curtiss, H.-G. Jung, S.M. Borisov, S.A. Freunberger og, Y.-K. Sun, Nat. Commun. 10 (2019) 1380.
[24] J. Kim, J. Lee, J. Jeong, C. Hwang og, H.-K. Song, Appl. Mat. Int. 14 (2022) 9066–9072.
[25] Y. Dou, D. Kan, Y. Su, Y. Zhang, Y. Wei, Z. Zhang og, Z. Zhou, J. Phys. Chem. Lett. 13 (2022) 7081–7086.
[26] K. Kim, J. Jeong, G. Jung, J. Lee, J. Lee, K. Baek, S. Kang, S. Kwak, C. Hwang og, H.-K. Song, Appl. Mat. Int. 14 (2022), 40793.
[27] J. Kim, G. Jung, C. Hwang, J. Jeong, K. Baek, J. Lee, S. Kang, S. Kwak og, H.-K. Song, J. Power Sources 492 (2021), 229633.
[28] C. Hwang, J. Yoo, G. Jung, S. Joo, J. Kim, A. Cha, J.-G. Han, N.-S. Choi, S. Kang, S.-Y. Lee, S. Kwak og H.-K. Song, ACS Nano 13 (2019) 9190–9197.
[29] R.F. Nelson, D.W. Leedy, E.T. Seo og, R.N. Adams, Z. für Anal. Chem. 224 (1) (1966) 184–196.
[30] W.-J. Kwak, H. Kim, H.-G. Jung, D. Aurbach og, Y.-K. Sun, J. Electrochem. Soc. 165 (10) (2018) A2274–A2293.
[31] M. Lee, J. Hong, B. Lee, K. Ku, S. Lee, C. Park og, K. Kang, Green Chem. 19 (2017) 2980.
[32] W.-J. Kwak, H. Kim, Y. Petit, C. Leypold, T. Nguyen, N. Mahne, P. Redfern, A. Curtiss, H.-G. Jung, S. Borisov, S. Freunberger og, Y.-K. Sun, Nat. Commun. 10 (2019) 1380.
[33] M. Orfanopolus, I. Smonou og, C. Foote, J. Am. Chem. Soc. 112 (1990) 3607–3614.
[34] D. Singleton, C. Hang, J. Szymanski, M. Meyer, A. Leach, K. Kuwata, J. Chen, A. Greer, C. Foote og K. Houk, J. Am. Chem. Soc. 9 (2003) 1319–1328.
[35] Y. Hayashi, S. Yamada, T. Ishikawa, Y. Takamuki, M. Sohmiya, H. Otsuska, K. Ito og M. Saito, J. Electrochem. Soc. 167 (2020), 020542.
[36] J. Uddin, V. Bryantsev, V. Giordani, W. Walker, G. Chase og D. Addison, J. Phys. Chem. Lett. 4 (2013) 3760–3765.
[37] R. Wyckoff, Crystal Structures, second ed., 1, Interscience Publishers, New York, London, Sydney, 1963.
[38] S. Mair, Acta Crystallogr. A34 (1978) 542–547.
[39] X. Yao, Q. Dong, Q. Cheng og D. Wang, Angew. Chem. Int. Ed. 55 (2016) 11344–11353.
[40] D. Kwabi, T. Batcho, C. Amanchukuwu, N. Oritz-Vitoriano, P. Hammond, C. Thompson og, Y. Shao-Horn, J. Phys. Chem. Lett. 5 (2014) 2850–2856.
[41] S. Freunberger, Y. Chen, N. Drewett, I. Hardwick, F. Bardé og, P. Bruce, Angew. Chem. Int. Ed. 50 (2011) 8609–8613.
[42] M. Ottakam Thotiyl, S. Freunberger, Z. Peng og, P. Bruce, J. Am. Chem. Soc. 135 (2013) 494–500.
[43] B. McCloskey, A. Speidel, R. Scheffler, D. Miller, V. Viswanathan, J. Hummelshøj, J. Nørskov og, A. Luntz, J. Phys. Chem. Lett. 3 (2012) 997–1001.